LOCALISED CORROSION SUSCEPTIBILITY OF AISI 304L (UNS S30403) STAINLESS STEEL WELDED JOINTS IN SEA WATER

[1]Iwuoha, A. U., [2]Isiohia, D. O., [2]Onyeka, J. O. and [3]Atanmo, P. N.

[1]Department of Mechanical Engineering, Imo State University, Owerri, Imo State, Nigeria.
[2]Department of Civil Engineering, Imo State University, Owerri, Imo State, Nigeria.
[3]Department of Mechanical Engineering, Anambra State University, Uli, Anambra State, Nigeria.
Email: [1]nmatoha@yahoo.com.

ABSTRACT

This study is on the susceptibility of AISI 304L austenitic stainless steel welded joints to localized pitting corrosion in sea water. AISI 304L is more resistant to corrosion primarily because of its low carbon content. This makes it less susceptible to welding sensitization. However, high power density welding techniques like electron beam or laser beam creates a narrow HAZ and with its rapid cooling leaves the Cr in solution for formation of Cr-oxide. The study compared the pitting resistance of welded joints [produced by SMAW and MIG] in two sea waters –one natural (of 4% dissolved salt content) and the other synthetic (of 8% dissolved salt content). All the studies were by immersion method. The WM and HAZ by MIG indicated higher pitting corrosion resistance in both environments, that of SMAW were found susceptible in both media, with higher pitting density in the greater salt-concentration environment. The near-high power density of MIG process succeeded in creating a narrow HAZ because of sharp thermal slope inherent in the technique. This was not the case for SMAW joints with extended HAZ and attendant $Cr_{23}C_6$ precipitation / Cr depletion. From this paper, AISI 304L welded joints made by MIG and service-deployed in sea water **(dissolved salt content < 8%)** handling facilities can be considered stable and "safe." The SMAW process sensitized the HAZ, and the regions of austenite / delta-ferrite interface was greater -hence the corresponding corrosion-weak sites. This negatively shifted the pitting potential of joints by SMAW.

Key Words: AISI 304L Stainless Steel, SMAW, GMAW (MIG), Pitting Corrosion, Chromium Depletion.

ABBREVIATIONS

AISI	American Iron and Steel Institute
API	American Petroleum Institute
ASM	American Society for Metals
ASNT	American Society for Nondestructive Testing
ASTM	American Society for Testing and Materials
AWS	American Welding Society
DCEN	Direct Current Electrode Negative
DCEP	Direct Current Electrode Positive
Ecp	Critical Pitting Potential
FN	Ferrite Number
ICC	Intercrystalline Corrosion
UNS	Unified Alloy Numbering System
WPS	Welding Procedure Specification

NOMENCLATURE GLOSSARY

Heat Treatment: This is the operation or combination of operations, requiring heating and cooling of a metal or metallic alloy in its solid state with the intention of changing the characteristics of the metal or alloy. A heat treatment cycle consists of three main stages: heating the material at a suitable pace, holding at an appropriate temperature for the desired time, cooling the metal or alloy at an appropriate pace.

Passivation: This is the selective dissolution of iron, nickel atoms from the surface layers of steel materials and oxidizes the left over chromium atoms thus forming a corrosion-resistant chromium oxide surface. Passivation is done with nitric acid or recently with heated citric acid solutions.

Pickling: This is the removal of surface oxides on steel (formed during welding or heat treatment), other surface contaminations such as bare iron and layers of metal deficient of chromium (due to heating sensitization) at immediate-undersurface of the material. The procedure for pickling is contained in ASTM A380.

Sensitization: This is the heating (whether intentional, accidental or coincidental) of steel or alloy steel which provokes precipitation of corrosion-resistant constituents at grain boundaries and thus make the material become less resistant or prone to corrosion at the grain or crystal boundaries.

Solution: This connotes the microstructure of the alloy steel. When the alloy steel is heated to about 700 ^{o}C and above in vacuum, air or in a protective environment, the carbides such as chromium carbides ($Cr_{23}C_6$) dissolve into the solid austenitic (in this austenitic structure, the metal atoms have a face-centered cubic [f.c.c.] microstructure) alloy, when this hot steel alloy is cooled quick enough, the carbon does not have the time to precipitate and go into the carbide phase with the corrosion inhibiting constituent. In this way, the carbon remains in solid form within the solid alloy (solid solution).

1.0 INTRODUCTION

Stainless steels (SS) are iron-based alloys containing a minimum of 10.5% chromium with or without other alloying elements (Rabbe and Heritier, 1999). “Stainless” refers to the resistance to staining, pitting and rusting in the general normal environment and some other defined corrosive media. This resistance to corrosion is by the formation, in the presence of oxygen, of an invisible and “sticking” chromium-rich oxide surface film which prevents further rapid oxidation of the metal. The strength, ease of welding and corrosion resistance are based on the alloy’s microstructure and this microstructure is in turn governed by the chemical composition of the alloy. The groupings of stainless steel are based on the predominant microstructure and are mainly: austenitic, Ferritic, martensitic, austenitic-ferritic (duplex) and precipitation hardening stainless steels. Austenitic SS is commonly used. This steel is alloyed with chromium, molybdenum, and at times copper and titanium. Usually, it also contains high content of austenite-formers, like nickel. Austenitic SS is extensively used in the food and beverage industry, salt water (sea water) handling equipment, hydrocarbon gas processing, nuclear and chemical industries. Failures of SS AISI / ASTM Type 304L have been reported severally in fire water pumps and pipe spools using sea water for fire emergencies in offshore installations.

AISI Type 304L austenitic SS is known for its better weldability and superior corrosion resistance quality than Type 304 due mainly to its low carbon content. This enables the making of high quality weldments with improved corrosion resistance in strong chloride bearing media (like sea water) and to sensitization especially in the heat affected zone (HAZ). Sensitization in the weld metal and HAZ results from $Cr_{23}C_6$ precipitation at the grain boundaries, depleting the region of Cr necessary for formation of CrO for inhibition of corrosion. This characteristics can further be improved with the use of welding process of high power density like the electron beam or laser beam welding (EBW or LBW). This type of welding process creates a narrow HAZ due to steep or high thermal slope generated by the process. Thus there is less susceptibility to formation of precipitates especially $Cr_{23}C_6$ and the pitting and intergranular corrosion resistance of the weld product is improved. For this study, the use of EBW or LBW was not within reach and the team opted to compare the corrosion potentials in welded joints produced by shielded metal arc welding (SMAW) and metal inert gas (MIG) welding. SMAW is the common conventional process. MIG with it shielding gas is rapid and has high metal deposition rate. With a heat dissipater around the HAZ, MIG process is near efficient like high energy density welding and thus a narrow HAZ and by extension, decreased susceptibility is expected.

2.0 THEORETICAL BACKGROUND

Corrosion Properties

Austenitic SS have high corrosion resistant properties in general corrosive environments. With increasing chromium, their corrosion resistance properties are enhanced especially in severe environments. Resistance to pitting and crevice corrosion in chloride-active media is very important since chlorides provoke corrosive

attacks. The strong chloride content of seawater prones SS particularly to pitting and crevice corrosion, this becomes severe with increase in service temperature (Samans, 2008).

Weldability of Austenitic Stainless Steels

Austenitic SS grade of AISI type 304 is generally excellently weldable. The problem commonly encountered is pitting and crevice corrosion of the weld metal in severe corrosion environments. Attempts have been made to solve this by use of low carbon content (< 0.04%) grades and inclusion of niobium and or titanium as stabilizers (preferential carbides formers) without adequate success (Santarini, 1999). Further, problem of hot cracking (which is weld cracking well before solidification is completed) is encountered when Cr content is increased. Weld metals of AISI 304 may undergo precipitation of $Cr_{23}C_6$ at the grain boundaries, thus depleting Cr and making the SS This information (properties of different phases present) from the diagram helps the metallurgist to estimate service life of the welded piece. The diagram can equally give guidance on the weldability of different SS grades. In some cases, deviations have been established from microstructure predictions based on the Schaeffler-De-Long diagram (Arioke, et al, 2006). Figure 2 refers to corrosion rate with oxidizing power for parent and sensitized crystal boundaries. For instance if the oxidizing power is between B and C, the parent metal will not corrode (because a passive film has been formed) but the grain boundaries will, thus we have preferential corrosion at the intercrystalline sites.

Welding Processes

Austenitic stainless steels can be welded with almost any electric arc welding process in addition to friction welding, laser beam, electron beam and resistance welding processes. The physical and metallurgical properties undergo changes during the weld process, these changes are significant enough compared with other SS and carbon steel. Compared with ferritic SS, the thermal expansion coefficient of austenitic stainless steels is about 135% greater and by extension, this means that distortions during welding may be more problematic. However, the heat conductivity of the austenite SS is about 50% that of the ferrites, to be preferentially susceptible to corrosion at the grain boundaries. There may also be the precipitation of the brittle sigma Fe-Cr phase in their microstructure if they are exposed to high temperatures for a certain length of time as experienced during welding. 700 - 850^{o}C is the temperature range where the transformation from ferrite to sigma or directly from austenite to sigma takes places the fastest. High heat input welding invariably leads to slow cooling. During this slow cooling time, the temperature range of 700 - 850^{o}C stretches in time and with it the greater formation of the sigma phase (Sedrika, 2008).

Theoretical Approximation of Welded Microstructures -Schaeffler-De-Long diagram

Schaeffler-De-Long diagram (Figure 1) helps in the approximate determination of the structural constituents in a weld metal.

then lower heat inputs can be used to obtain same weld penetration and thus minimize weld distortions. Another difference is that the weld pool of austenite SS is more viscous than the ferrite and as such, wetting problem may ensue.

Notably, the common problems associated with welding austenitic SS are solidification and liquation cracking (hot cracking) and $Cr_{23}C_6$ precipitation at the grain boundaries. For cracking, this is the result of segregation of certain elements to the liquid phase during solidification, this segregation leads to the presence of low melting point layers at the junction between the solidification fronts, usually at the interdendritic regions in the longitudinal plane where the weld midline is situated. (Pinnow, and Moskowitz, 1980). At cooling, residual stresses pull these apart. The internal surfaces of these cracks so created have blue coloration because of minor oxidation of the surfaces. Since the presence of ferrites positively shifts the hot cracking phenomenon, ferrites are included in the welds to achieve this.

In principle, to overcome most of these problems, high quality welds in austenitic SS can be made if they are heated to high temperature for a very short time; they are completely protected from the atmosphere during welding and the welding is done at a high rate. Also, to avoid heavy residual strains and other effects detrimental to the

weldment common with conventional welding methods (where there is relative low concentration of energy), highly concentrated heat rate process is used. Here Electron beam welding and laser beam welding come to mind.

Intercrystalline Corrosion (ICC) or Intercrystalline Attack (ICA)

Intercrystalline or intergranular corrosion is a form of corrosion which primarily affects the grain boundaries of a polycrystalline metal. The process is rapid with initial little metal loss but it leads to the breakdown of crystalline cohesion, hence grain dissociation with eventual grain disintegration. The most important basis for this intercrystalline corrosion is the material itself or the material composition. Major examples of materials prone to this type of corrosion are the highly alloyed austenitic chromium-nickel and ferritic chromium steels. When austenitic steel has been exposed for a time in the temperature range of approximately 550 ^{o}C to 750 ^{o}C, or when the steel has been heated to higher temperature and allowed to cool slowly through that temperature range (such as occurs after welding or air cooling after furnace annealing), the chromium and carbon in the steel matrix have time, and do combine to form chromium carbide particles with the formula $Cr_{23}C_6$ along the grain boundaries. These precipitate chromium carbide particles are formed with the chromium in that region and thus cause it to be deficient in chromium required for corrosion resistance allowing the steel to corrode preferentially along the grain boundaries. Steel in this condition is said to be "sensitized", i.e. sensitive to corrosion. It should be noted that carbide precipitation depends upon carbon content, temperature and time at temperature. The most critical temperature range is around 700 ^{o}C, at which 0.07% carbon steels will precipitate carbides in about 2 minutes, whereas 0.02% carbon steels are, in some cases, reported to be effectively immune from this problem (Clerke et al., 2006). Titanium and niobium each has much higher affinity for carbon than chromium and therefore titanium carbides, niobium carbides and tantalum carbides form instead of chromium carbides, leaving the chromium in solution and ensuring full corrosion resistance. In cases where corrosion is not an issue but strength at elevated temperatures, the presence of grain boundary carbides is not harmful to the strength of stainless steels. Grades meant for this service are deliberately "topped-up" with high carbon content and such grades include 304H, 316H and 347H (Yang, 2000).

The time, temperature and carbon factors affecting the intercrystalline corrosion are graphically illustrated in the Time Temperature Sensitization (TTS) diagram (Figure 3) below.

Pitting Corrosion

This type is marked by stand-alone cavities that are mostly hemispherical in shape. They progress inwards gradually in the affected spot and could lead to eventual perforation of the metal while the bulk of the metal surface shows no corrosion. Pitting corrosion is commenced by the presence of chlorides. It occurs frequently in stagnant solutions and aggravated by increasing temperatures. The mechanism is that of local degradation of the passive layer on the metal surface which leads to a small corrosion anode on that spot, while the oxygen reduction can proceed freely on the large passive area. This introduces or effects a very significant drop in the pH value of the fluid trapped in the already formed cavity as a result of hydrolysis of the corrosion products. The point to note is that all passivatable materials are prone to pitting corrosion and the austenitic stainless steels fall within this grade. Molybdenum additive to the stainless steel helps to arrest this; the quantity of molybdenum is increased with increase in chloride content and rise in service temperature.

3.0 METHODOLOGY

AISI 304L SS material of 7.75 mm thickness was sourced from the field and the chemical composition analysis performed to confirm the constituents of the material (Table 1). The material was prepared (cut) into 40 pieces of 50 x 50 x 7.75 mm each. The pieces were paired into abutting single V-groove joints and welded: 10 pairs were welded with shielded metal arc welding (SMAW) process and the other 10 pairs were welded with metal inert gas welding (MIG) process. Each of the two processes was done with welding electrodes containing carbon % by mass fraction compatible with that of base metal. The

details of the welding conditions are shown in Table 2. The welding workmanship was from a WQR pool prepared in a shop of similar services. The WQR was prepared the past three (3) months prior this studies. The WPS used was previously prequalified for fire water pump pipe spools (AISI 304L grade) on duty 3 metres in sea water; the same service conditions for the weldments. AWS B2.1: *Standard for Welding Procedure and Performance Qualification* is the reference standard for welding procedure specifications.

The 10 pieces welded per SMAW were partially dissolved in 10% HCl-methanol mixture to remove slag particles trapped in the weldments. Each welded specimen had a 10 mm hole **(to enable tie a marine rope to the specimen)** bored through it at a suitable point at one of the square corners. The specimens were then ground and polished to fine diamond grade after which they were pickled and rinsed with de-mineralized water. This was done to remove fully the oxide and chromium-depleted layers in the specimens. Due care was taken to avoid stain or inadvertent corrosion on the surfaces. (Hopkin, G. J., 2001). Components that have been correctly ground, pickled and rinsed will normally have better corrosion resistance than surfaces that were ordinarily brushed or machined. (Maiya, P. S., 1989).

Corrosion Studies

Natural Sea Water

From each welded process, five (5) specimens were separately immersed into sea water (salt content calculated at 40,000 ppm [4% dissolved salt]) to a depth of 1 m and each tied to a wooden brace in a concrete jetty in Akwa Ibom State, Nigeria serving a local community in a beach front of the Atlantic water. The concrete jetty was constructed and put into use about 9 months before this investigation. The specimens were protected in an area by marine rope netting and were allowed in the immersed state for 120 days. This is to allow enough time to grow the pits (if any) for shape studies. To study the initiation sites of the pits, the pitted weld metal specimens were etched in 10% ammonium persulphate, cleaned, dried, and first observed visually and later examined in an optical microscope.

Synthetic Sea Water

The sea water as used above was collected into a plastic container, 40 gram/litre sodium chloride (NaCl) was added proportionately to it to achieve 80,000 ppm [8% dissolved salt content]. This new corrosive medium (synthetic sea water) is naturally aerated at ambient temperature and was intended to have salinity greater than the natural sea water earlier used. The synthetic sea water was divided into two separate plastic containers; each weld process remaining specimens (5 pcs each) were then immersed into the synthetic sea water –each weld process specimens into a separate container. The immersion was allowed to stand for ninety (90) days. At the end of the duration, the specimens were retrieved, cleaned, dried, and first observed visually. Metallographical studies with Villela's reagent was done to analyze the microstructure of sites of pits initiation and growth (ISO 11130:1999, ASTM G31:2004 and ASTM G52:2004).

Another procedure for this test would be the tests of ASTM E975 (ASTM, Annual Book of ASTM Standards, 2006)). *This requires use of x-ray diffraction technique to measure and quantify the austenites, ferrites, sigma and chi phases in the weld metal. Thereafter, pitting potential determinations will be made using potentiodynamic polarization measurements, conducted using NaCl electrolyte and platinum counter electrode and saturated calomel reference electrode. The series of corrosion potentials (E_{corr}) generated will be interpreted as suggested by Fontena and Stachle, 2007.*

4.0 RESULTS AND ANALYSIS

Microstructures

Figure 4 shows the microstructure of the base metal (BM) before the weld, which is mainly austenitic with some retained ferrite. Figures 5 and 6 show the microstructures of the weld metal (WM) and HAZ of specimen welded by SMAW. Figures 7 and 8 show the microstructures of WM and HAZ obtained from MIG. The HAZ microstructure from SMAW is, expectedly heterogeneous due to gentle thermal slope established by the weld process with some delta-ferrite stingers in line with the rolling direction of the plate. The microstructure is still austenitic but

not ferrite-free, the transformations that have occurred –some of which is micromartensitic- have reduced the quantity of austenite and introduced thermal stress. The different microstructures present could only be identified and quantified by Transmission Electron Microscopy (TEM). This could not be done because of equipment unavailability. The microstructure of HAZ from MIG is not as inhomogeneous as identified in that of SMAW. This is explained as due to the near-high energy rate density associated with the process which created a steep thermal gradient in the HAZ (a narrow HAZ strip) –hence the microstructure is close to that of the BM, with delta-ferrite next to the fusion line. In the MIG joint, the WM cooled and solidified quick enough, has in its microstructure "quenched" austenite and delta-ferrite with some measure of delta-ferrite transformation to secondary phases. The quick cooling equally introduced thermal strains. In this matrix, the Cr remains in solution to form a passivation oxide when exposed to oxidizing corrosive medium. According to other researchers (Rodriguez, et al, 1999), retained ferrite has no effect on pitting susceptibility, though it is well established that this phase encourages the dissolution of carbon and progressive formation of carbide precipitates and by extension more available sites for pit nucleation / growth. However, the results by some other researchers (Robinson and Scully, 2000) showed that increase of ferrite content positively shifts the pitting potential. From basic metallurgical perspective, this is not expected except in cases where the BM is martensitic. The phenomenon requires further investigative studies to draw vivid conclusions. The results of this investigation support the former researchers.

Localized Corrosion

Natural Sea Water (40,000 ppm Salt Content)

SMAW WM and HAZ: All the retrieved specimens indicated noticeable pits and the metallography performed showed the initiation sites dominantly in the HAZ. This confirms the depletion of Cr in that zone required for Cr-oxide passivation. The photomicrograph (Figure 9) of some of the specimens indicated pits more in the HAZ than in the WM. This is due to weld heat sensitization of the HAZ –it promoted the combination of Cr and carbon to form $Cr_{23}C_6$ mainly at the grain boundaries, thus Cr is depleted. In the WM, transformation of delta-ferrite to secondary phases like the brittle sigma is effected. This effectively reduced the regions of austenite / delta-ferrite interface and correspondingly the corrosion-weak sites in WM compared to the HAZ. In the HAZ, the presence of delta-ferrites increases pit susceptibility because it promotes formation of Cr-depletion zones by precipitation of carbides.

MIG WM and HAZ: The specimens indicated no signs of pitting corrosion. The three regions of the specimens, i.e. WM, HAZ and nearby BM indicated surfaces free from any form of corrosive attack. The WM, as has been noted earlier has a "quenched" austenite microstructure created by the welding process. It is however noted that in situations of rapid cooling as this, insufficient time is available for complete mixing and diffusion of the elements in the weld pool. As such, after cooling, there exists tiny regions that are more highly alloyed than the bulk WM. These regions are harder and in service could be problematic with respect to stress corrosion cracking. Annealing ameliorates this but in cases of non-annealing of the weldment, the hardness via some mechanisms, is "managed" around 240 – 260 Hv. (Folkhard, 1998).

Synthetic Sea Water (80,000 ppm Salt Content)

SMAW WM and HAZ: All specimens showed visible marks of pitting corrosion. The photomicrograph (Figure 10) of one of the specimens showed wide and deep pits with effects of *Tuberculation* on the surface of the weldment. Pits appeared to originate randomly from all parts of the weldment microstructure (higher pit density) and the relatively large size of pits makes it further difficult to determine which part of the weldment the pit nucleated from and grew. Because of the gentle heat slope, re-dissolution of the carbides will not be achieved and Cr-carbide precipitates will be formed and initially, the pits will preferentially initiate from the HAZ where the degree of sensitization is higher.

MIG WM and HAZ: The pitting resistance showed in the natural sea water was also observed in the synthetic sea water of double salt content i.e. more corrosive medium compared with the natural sea water. All the three regions of interest of the welded joints indicated no signs of pitting corrosion. Upon close observation, the WM showed the highest resistance to staining -as a result of the "quenched" austenite microstructure compared with WMs of SMAW process, MIG produces superior WMs with respect to pitting resistance. It is noted that MIG process (because of the steep heat gradient in the HAZ) will produce different microstructural changes in different steel compositions particularly due to the Cr content. The HAZ has nobler resistance to pitting than the BM and the explanation is because of the re-dissolution of the Cr-carbides which frees up and increases the Cr content in solid solution matrix (Espy, 1982).

Another group of researchers (Robinson, 2008) performed similar investigations but in a laboratory where the test specimens for the electrochemical experiments were mounted in a polyester resin and pitting potential determinations were made using potentiodynamic polarization measurements. The electrolyte was a 4.85% mass reagent-grade sodium chloride in distilled water and was aerated naturally at 26^{o}C. The results of the measurements were translated into polarization curves for each of the regions of WM, HAZ and BM. The curves were then mapped into pitting potentials. For the MIG joints, none of the curves showed active-passive transition, the deduction here is that the regions were passivated in the electrolyte. This is supported by the low current initially. As the pitting potential increased, an oscillation manifested which is explained as due to nucleation and metastable growth mechanisms that were soon repassivated. It was noted that the repassivation took place at lower current, below the pitting potential. This gradually decreased as the number of sites open for pit initiation became unavailable. These results support the findings from our own investigations.

CONCLUSIONS

1. MIG process created superior (compared with SMAW) WM and HAZ welded joints that are quite resistant to corrosion pitting in sea water of up to 80,000 ppm salt content i.e. 8% dissolved salt content. These joints are considered stable and can safely be deployed in Nigeria offshore sea water handling facilities. The weld mechanism created a sharp thermal slope which "inhibited" sensitization in the HAZ. The stable microstructure in the WM retained Cr in solid solution and will quickly form passive Cr-oxide film.
2. SMAW mechanism produced AISI 304L welded joints that are very susceptible to localized pitting in the welded joints. The joints are not suitable for sea water service in Nigeria offshore environment and any other sea water of > 10,000 ppm of dissolved salt content. They may be used for services in the Baltic Sea with 0.7% dissolved salt content.

ACKNOWLEDGMENTS

We acknowledge discussions with Dr. A. N. Okpala of Niger Delta University. Acknowledgment is also due to the Engineering team of Standards Organisation of Nigeria, Enugu Engineering Laboratory for their interest and assistance during the studies, Offshore Pipeline and Welding Services for assistance in this work. Finally, we thank Mr. D. C. Etebi for taking the photomicrographs.

REFERENCES

American Welder, (2002), Welding Journal: Keep it Safe, Welding Fumes and Gases, Welding Journal, Vol.81, No.9, Supplement: The American Welder, pp 106.

Arioke, A., Yamada, T., Tesachi, T. and Staechle, R. W., (2006), Intergranular Stress Corrosion Behaviour in Austentic Stainless Steel in Hydrogenated High-Temperature water, NACE Corrosion Journal, PP 74.

Atteridge, D. G. et al., Sensitization and IGSCE Susceptibility Prediction in Stainless Steel Pipe Weldments, Conference Papers NO, 42, NACE, Houston, Houston, Texas, 1999.

ASM, (1994), ASM handbook Vol 6 - Welding, Brazing and Soldering, ASM, Ohio, ISBN 0-87170-382-3.

ASM., (1994), ASM Speciality Handbook - Stainless Steels, ASM, Ohio. ISBN 0-87170-503-6.

ASTM G31, (2004), Recommended Practice for Laboratory Immersion Corrosion Testing of Metals, Philadelphia.

ASTM G52, (2004), Recommended Practice for Conducting Surface Sea Water Exposure Tests on Metals and Alloys, Philadelphia.

AWS B2.1, 2004: Standard for Welding Procedure and Performance Qualification, American Welding Society, Miami, Florida.

Cieslak, W. R., Duquette, D. J. and Savage, W. F., (1991), Pitting Corrosion of Stainless Steel Weld Metals, Proceedings of Trends in Welding Research in the United States, David, S.A., ed. Materials Park, OH: ASM.

Clarke, S., (2000), Stress Corrosion Cracking of Stainless Alloys in Oxygenated Caustic Environments, Paper presented at Corrosion 2000, 55th Annual Conference and Exposition, Orlando, Florida, USA. 26-31, March 2000. Paper No. 00596, NACE International, Houston, Texas.

Clerke, W. L., Cowen, R. L. and Walker, W. L., (2006), Intergranular Corrosion of Stainless Alloys, ASTM 655, Philadelphia, P.A.

Cragnolino, G., Dunn, D. S. and Sridherhas, N., Environmental factors in the stress corrosion cracking of Type 316 Stainless Steel in chloride solutions.

DeLong, W. T., Ostrom, G. A. and Szumachowski, E. R., (1956), Measurement and Calculation of Ferrite in Stainless Steel Weld Metal, Welding Journal, Vol.35, No.11.

Downs, D. L., (2001), Uphill Diffusion of Carbon at Dissimilar Metal Junctions, Ph.D. Thesis, Hughes Hall, University of Cambridge.

Espy, R. H., (1982), Weldability of Nitrogen-strengthened Stainless Steels, Welding Journal, Vol.61, No.5, pp.149s-156s.

Folkhard, E., (1998), Welding Metallurgy of Stainless Steels, Springer-Verlag, Wein. ISBN 0-387-81803-0.

Fontena, M. G. and Stachle, R. W., eds., (2005), Advances in Corrosion science and Technology, 3. Plenum press, New York, PP.369.

Gill, T. P. S., Vijayalakshmi, M., Gnanamoorthy, J. B. and Padmanabhan, K. A., (1986), Welding Journal, 66.

Hopkin, G. J., (2001), Modelling Anisothermal Recrystallization in Austenitic Stainless Steels, Ph.D. Thesis, Fitzwilliam College, University of Cambridge. www.msm.cam.ac.uk/phase-trans/

Horowitz, H., (1998), Welding, Principles and Practice, Houghton Mifflin, Boston. ISBN 0-395-24473-0.

ISO7539-1: 1987 Corrosion of Metals and Alloy Stress Corrosion Testing – Part 1: General Guidance on Testing Procedures.

ISO 11130:1999, Corrosion of Metals and Alloy – Alternate Immersion Test in Salt Solution.

ISO 3651-1:1998, Determination of Resistance to Intergranular Corrosion of Stainless Steels – Part : Austenitic and Ferritic-Austenitic (Duplex) Stainless Steels – Corrosion Test in Nitric Acid Medium by Measurement of loss of Mass. (Huey Test).

ISO 3651-2:1998, Determination of Resistance to Intergranular Corrosion of Stainless Steels – Part 2: Fertitic, Austenitic and Ferritic – Austenitic (Duplex) Stainless Steels – Corrosion Test in Medium containing Sulphuric Acid.

Kamachi Mudali, U., Gill, T. P. S., Seetharaman, V. and Gnanamoorthy, J. B., Proceedings of National Welding Seminar, NWS-86 Indian Institute of Welding, Bombay, 1986.

Maiya, P. S., Corrosion 45 1989: p. 900.

Nishimoto, K., Matsunaga, T., Tanaka, T. and Okazaki, T., (1998), Effect of Bismuth on Reheat Bracking in a Type 308 FCA [Flux Cored Arc] Weld Metal, Welding in the world/Soudage dans le monde, Vol.41, No.3, pp.220-235.

Pinnow, K. E. and Moskowitz, A., (1980), Welding Journal, 49, New York.

Rabbe, P. and Heritier, J., (1999), Properties of Austenitic Stainless Steels and their Weld Metals, Influence of Slight Chemistry Variations, ASTM STP 679.

Raquet, O., (1994), Quantitative Characterization of Initiation and Propagation in Stress Corrosion Cracking: An Approach of a

Phenomenological Model, Ph.D. Thesis, University of Bordeaux, France.

Raquet, O., Hélie, M. and Santarini, G., (1994), Initiation and Propagation in Stress Corrosion Cracking, Materials Week, 1994, Rosemont, Illinois.

Robinson, J. L., (1979), Preferential Corrosion of Welds, Welding Institute Research Bulletin, Vol 20.

Robinson, M. J. and Scully, J. C., (1977), Stress Corrosion Cracking and Hydrogen Embrittlement of Iron-Based Alloys, NACE-5, Staehle, R.W., Hochmann, J., McCright, R. D. and Slater, J. E., eds., NACE, Houston.

Rodriguez, P., Bhattacharya, D. K. and Mannan, S. L., (1976), Welding of Stainless Steels, Proceedings of Indian Institute of Welding Seminar, Indian Institute of Welding, Bombay.

Samans, C, H., (2008), Stress Corrosion Cracking Susceptibility of Stainless Steels and Nickel-base Alloys in Polythionic Acids and Acid Copper Sulphate Solution, Corrosion, Vol. 20, No.8, pp.256t-262t.

Santarini, G., (1999), Corrosion 45.

Schaeffler, A. L., (1949), Constitution Diagram for Stainless Steel Weld Metal, Metal Progress Vol. 56 No.11 pp. 680-680B.

Sedrika, A. J., (2008), Corrosion of Stainless Steels, John Wiley and Sons, New York.

Snykess, M., Bogoerts, W., Bruggeman, A., Embrechts, M., Daenner, W. and Dr Steiner, (2002), Fusion Engineering Design 8, McGraw-Hill Books.

Solomon, H. D. and Lord, D. C., (2000), Corrosion, John Wiley and Sons, New York.

Standard Practices for Detecting Susceptibility to Intergranular Attack in Austenitic Stainless Steels, (2006), Annual Book of ASTM Standards, Vol. 03.02 Philadelphia, PA: ASTM.

Thomas, R. G. and Yapp, D., (1978), Welding Journal 57.

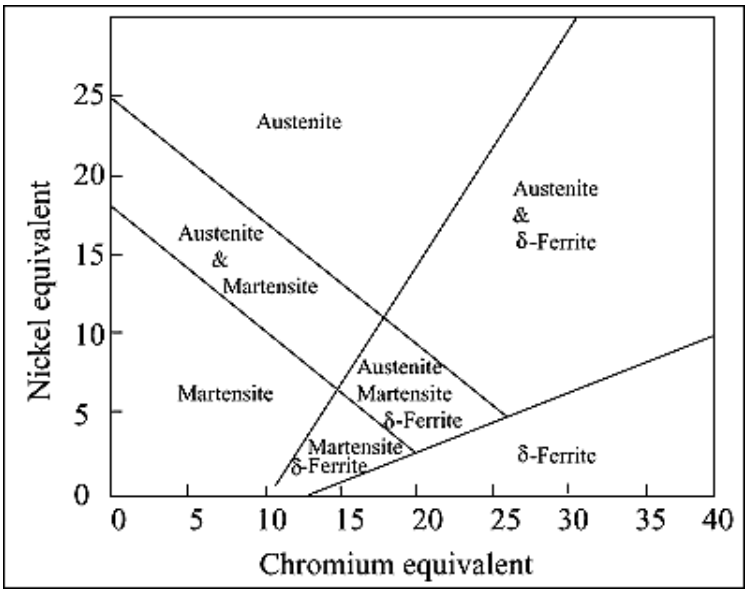

Figure 1: Schaeffler diagram: Basic effect of alloy additions on the Microstructure of Cr-Ni Alloys.

Source: *Schaeffler, A. L., (1949), Constitution diagram for stainless steel weld metal, Metal Progress.*

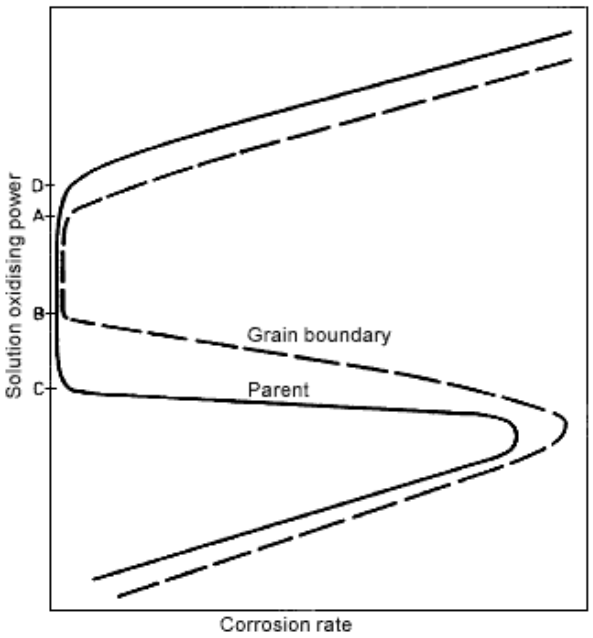

Figure 2: Solution oxidizing power versus corrosion rate for both base and sensitized grain boundary material.

Source: *Robinson, J. L., (1979): Preferential corrosion of welds, Welding Institute Research Bulletin, Vol 20.*

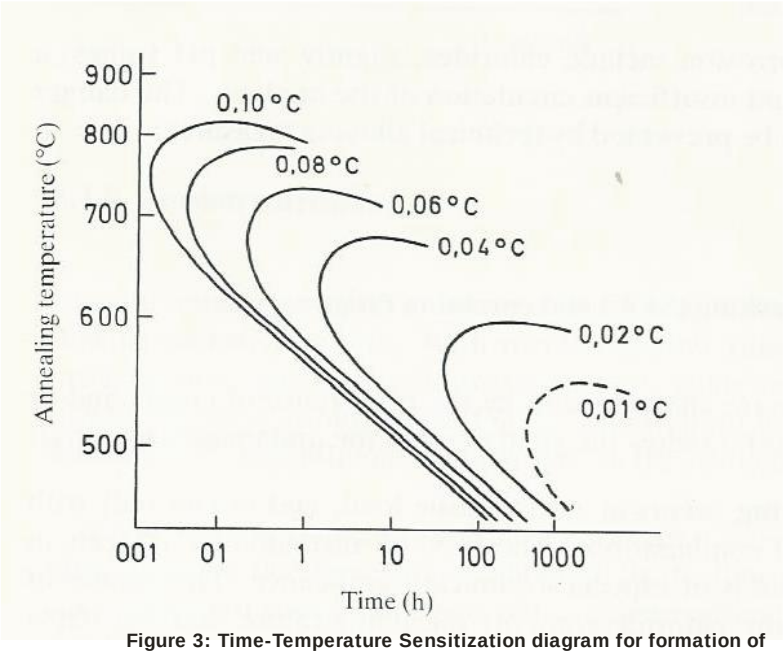

Figure 3: Time-Temperature Sensitization diagram for formation of harmful amounts of Cr-carbides in Stainless Steels as a function of Carbon Content.

Source: Solomon, H. D. and Lord, D. C., Corrosion, New York, 2000.

Table 1: Chemical Composition of AISI 304L (S30403) Stainless Steel Material and Welds Filler Materials.

Element	AISI 304L Stainless Steel Material (% by weight)	SMAW Weld Filler Material (% by weight)	GMAW Weld Filler Material (% by weight)
Carbon	0.03	0.028	0.028
Chromium	19.50	19.00	19.00
Nickel	11.50	11.50	11.50
Manganese	2.00	1.95	1.95
Silicon	1.00	1.15	1.15
Molybdenum	0.00	0.00	0.00
Phosphorus	0.045	0.04	0.04
Sulphur	0.03	0.005	0.005
Iron	Remainder	Remainder	Remainder

Table 2: Specimens Welding Conditions.

Welding Parameter	Welding Process	
	Shielded Metal Arc Welding (SMAW)	Gas Metal Arc Welding (GMAW/MIG)
Welding Technique	Direct Current Straight Polarity (DCSP)	Direct Current Straight Polarity (DCSP)
Welding position	Vertical-Up	Vertical-Up
Joint configuration	Single V, 60º	Single V, 60º
Root opening	1.0 mm	1.0 mm
Electrode type	E308L (AWS A5.4, A5.9 and A5.22)	ER308L (AWS A5.4, A5.9 and A5.22)
Electrode diameter	4 mm	4 mm
Pressure of gas (Argon)	Not Applicable	30 bar
Arc voltage	20 V	26 V
Welding current	150 A	170 A
Baking temperature	160 ºC for 1 hr.	200 ºC for 1 hr.
Inter-bead temperature	150 – 200 ºC	150 – 200 ºC
Number of beads	6	6

Figure 4: Microstructure of base metal (BM) before the weld -mainly austenite with retained ferrite.

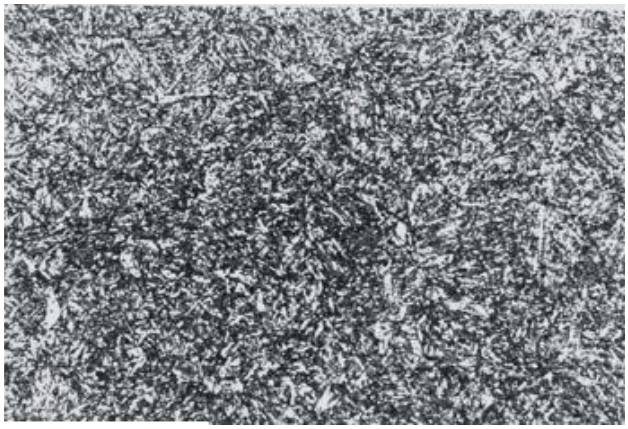

Figure 5: Microstructure of WM from SMAW.

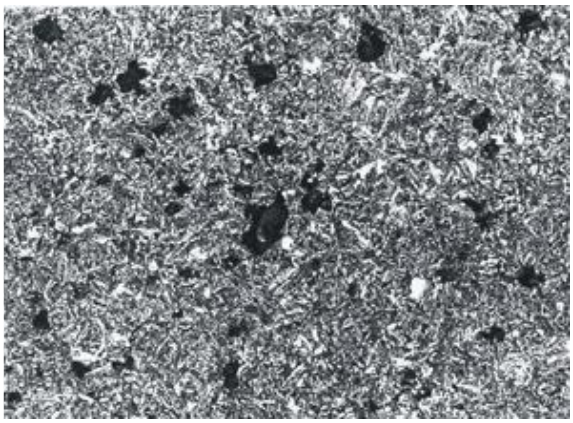

Figure 6: Microstructure of HAZ from SMAW -Heterogeneous austenite with some delta-ferrite stingers in line with the rolling direction of the plate.

Figure 7: Microstructure of WM from MIG. WM cooled quick enough, has in its microstructure "quenched" austenite and delta-ferrite with some measure of delta-ferrite transformation to secondary phases.

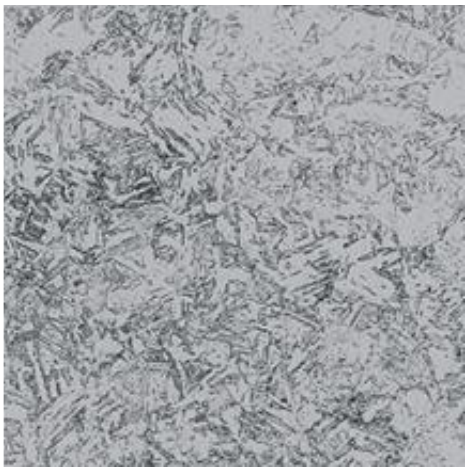

Figure 8: Microstructure of HAZ from MIG. This is not as inhomogeneous as identified in that of SMAW. The near-high energy rate density created a steep thermal gradient in the HAZ (a narrow HAZ strip). Microstructure is close to that of BM with delta-ferrite next to the fusion line.

Figure 9: Pitting Corrosion (Narueal Sea Water) on SMAW Welded Joint -Dorminantly in HAZ

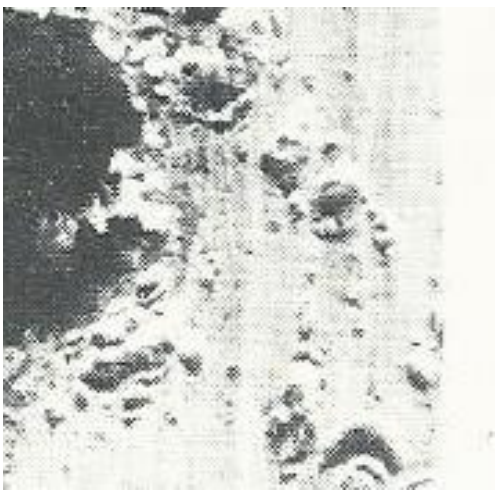

Figure 10: Pitting Corrosion (Synthetic Sea Water) on SMAW Welded Joint -Wide and Deep Pits originate randomly from all parts of Weldment Microstructure (Higher Pit Density).